A microscopic time scale approximation to the behavior of the local slope on the faceted surface under a nonuniformity in supersaturation

Etsuro Yokoyama*
Computer Center, Gakushuin University
Mejiro 1-5-1, Toshima-ku Tokyo 171-8588, Japan

Yoshikazu Giga†
Graduate School of Mathematical Sciences, The University of Tokyo
Komaba 3-8-1, Meguro-ku Tokyo 153-8914, Japan

Piotr Rybka‡
Faculty of Mathematics, Informatics and Mechanics, The University of Warsaw
ul. Banacha 2, 02-097 Warszawa, Poland

November 28, 2007

Abstract

The morphological stability of a growing faceted crystal is discussed. It has been explained that the interplay between nonuniformity in supersaturation on a growing facet and anisotropy of surface kinetics derived from the lateral motion of steps leads to a faceted instability. Qualitatively speaking, as long as the nonuniformity in supersaturation on the facet is not too large, it can be compensated by a variation of step density along the facet and the faceted crystal can grow in a stable manner. The problem can be modeled as a Hamilton-Jacobi equation for height of the crystal surface. The notion of a maximal stable region of a growing facet is introduced for microscopic time scale approximation of the original Hamilton-Jacobi equation. It is shown that the maximal stable region keeps its shape, determined by profile of the surface supersaturation, with constant growth rate by studying large time behavior of solution of macroscopic time scale approximation. As a result, a quantitative criterion for the facet stability is given.

Key words: facet instability, Hamilton-Jacobi equation, viscosity solution, macroscopic time scale approximation, maximal stable region

Email address: yokoyama@gakushuin.ac.jp, phone +81-3-5992-1048, fax +81-3-5992-1018
†labgiga@ms.u-tokyo.ac.jp,
‡rybka@hydra.mimuw.edu.pl

1 Introduction

We are preoccupied with the morphological stability of a growing faceted crystal. In order to put our task in a broader prospective we may say that we work within a Burton-Cabrera-Frank type model[1]. A modern derivation of a hierarchy of such models was done by E and Yip, [2], who obtained a Hamilton-Jacobi equation essentially the same as our (2.4). While the papers like [2, 3, 4, 5] and other ones deal with the behavior of the whole growing crystal treating peaks as rarefaction waves and valleys as shocks, we concentrate on a single fixed peak – a corner which is a step source with a constant in time vertical growth rate. We apply the approach as in Chernov's work [6] to study the morphological stability of a growing faceted crystal in which the interplay between nonuniformity in supersaturation on a growing facet and anisotropy of surface kinetics derived from the lateral motion of steps leads to a faceted instability, *i.e.*, the preferred growth of corners and edges of the faceted crystal, [7, 8, 9, 10]. We may summarize the conclusion of these articles by saying that as long as the nonuniformity in supersaturation on the facet is not too large, it can be compensated by a variation of step density along the facet and the faceted crystal can grow in a stable manner. However, there is no study how the compensating distribution of steps in time along the surface develops from an initial plane under nonuniformity in supersaturation.

The molecularly smooth surfaces cannot grow without the surface kinetic processes, such as the lateral motion of steps and the generation of steps. The surfaces of a growing polyhedral crystal inclined by a local slope p from the singular face, which is molecularly smooth, are composed of a parallel array of steps that are distributed with a mean step separation $\lambda = d/p$, where d is the step height. The dimensionless growth speed V in the direction normal to such a surface is generally expressed using the surface supersaturation σ and the dimensionless kinetic coefficient $m(p)$ as [1, 7]

$$\begin{aligned} V &= m(p)\sigma \ , \\ m(p) &= \frac{p}{p_s}\tanh(\frac{p_s}{p}) \, , \\ p_s &= d/2x_s \, , \end{aligned} \tag{1.1}$$

where x_s is the mean surface diffusion distance of a molecule on the surface, so p_s is a criterion of local slope, generally, the order of p_s is 10^{-2}.

The kinetic coefficient m in the form of (1.1) is valid outside the region where there are no step sources. At the step source we postulate that the position of the surface at supersaturation σ_0 moves upward with speed:

$$V_0 = s(\sigma_0)\tanh(\frac{1}{s(\sigma_0)})\,\sigma_0 \, , \tag{1.2}$$

where $s(\sigma_0)$ is the local slope of a growth hillocks formed by a two-dimensional nucleation or with the aid of screw dislocations. The functional form of $s(\sigma_0)$ depends on the growth mechanism, *i.e.*, two-dimensional nucleation growth or spiral growth with the aid of screw dislocations or [11].

Now, we describe our setting: we take a cross-section orthogonal to the edge of the surface and denote it by an interval $(0, L)$ where the step source is located at the origin. We consider a quasi-steady situation when the supersaturation equilibrates much faster compared to the motion of the steps. Moreover, in order to simplify the problem and avoid the

unnecessary difficulties related to solving the diffusion equation we assume that the supersaturation σ is a given function. Its main property is due to Berg's effect[12] [13], *i.e.*, σ is a decreasing function of the distance along the crystal from the origin. We consider a continuum limit of the step motion (see [2, 5, 7, 8, 9, 10]) this yields a Hamilton-Jacobi equation for the height of crystal over initially flat surface, see (2.4). In fact, this is a first order partial differential equation which describes a nonlinear step flux conservation.

Our main results imply that there exists a region of stable growth, *i.e.*, macroscopically flat region $(0, x_c)$, where x_c is a critical point so that the crystal shape in $(0, x_c)$ is asymptotically translation of a fixed profile with the same growth rate at the origin. The critical point x_c depends on σ. If σ is constant, we may set $x_c = L$ for any L. In this case any flat crystal surface stays macroscopically flat and it is stable no matter how large the crystal is.

What we do here is we solve the resulting equation numerically as well as we perform its rigorous theoretical analysis. In order to solve (2.4), we apply two methods: 1) we solve numerically the characteristics equation and 2) we solve (2.4) directly by using upwind differencing.

Our theoretical analysis is based on the introduction of fast time scale (later we will call it the *microscopic time scale*) related to a microscopic length parameter, $\varepsilon \approx p_s$, called the criterion of the local slope. We are able to link the full model (2.4) with ε appearing in the Hamiltonian H^ε to the microscopic time model (3.3) by the theory of viscosity solutions. Moreover, the problem of studying the asymptotics when ε goes to zero is replaced by the time asymptotics for (3.3), which is a fast growing subject. Interestingly, the situation we consider is not covered by the setting considered in [14, 15].

Moreover, we are able to justify rigorously the criterion of stable growth by Chernov, [7]. Our results show that the asymptotic behavior of local step density can be determined by the variation of reciprocal of supersaturation under the conditions of stability in the region $x < x_c$. There is, however, another approach to the problem of the stable growth of crystals, which is based upon the energetic approach. Rigorous results in this directions can be found in [16]. It would be very interesting to compare the respective notions of stable growth and the predictions about the size of stable facets.

The layout of this paper is as follows: in Section 2, we describe in detail the problem of growing faceted crystal under a given supersaturation. In Section 3, we introduce the microscopic time approximation and we justify the relation to the full model. in Section 4, we show explicit solution which lead to Chernov's stability criterion. In Section 5, we present the numerical results.

2 Growth rate equations based on step motion

We begin by considering a cross section of growing faceted crystal of length L. The interface of the growing facet is given by the function $z = u(x, t)$, where x and z are the coordinates parallel and normal to the facet, respectively, t is time, and the origin is at the left end of facet, where a step source is located. The local slope, p, is expressed by the partial derivative of u with respect to x and the growth rate perpendicular to x–axis, u_t, the partial derivative of u with respect to t.

The normal growth rate at the surface is given by

$$V(x, t) = m(p)\sigma(x)\,,$$

where $\sigma(x)$ is the supersaturation on the surface at point x and $m(p)$ is a kinetic coefficient

which depends on the step density *i.e.*, local slope p. It is, however, less convenient to work with V than with u_t, the growth rate perpendicular to x–axis. The shear geometry of the problem yields

$$u_t = m(u_x)\sqrt{1+u_x^2}\,\sigma(x) \quad \text{with} \quad p = u_x. \tag{2.1}$$

After specifying the growth rate of the step source using (1.2), the boundary condition at $x = 0$ becomes

$$\begin{aligned} u(0,t) &= ct\,, \\ c &= \frac{\sigma_0}{\varepsilon}\tanh(\frac{\varepsilon}{\sigma_0})\,\sigma_0 \end{aligned} \tag{2.2}$$

and we assume that the initial crystal surface is flat,

$$u(x,0) = 0\,. \tag{2.3}$$

The growth speed c equals V_0 defined in (1.2), where $s(\sigma_0)$ is taken so that $s(\sigma_0) = \sigma_0/\varepsilon$.

Thus, in fact (2.1) is in fact a Hamilton-Jacobi equation, whose Hamiltonian depends upon ε, because of (2.2):

$$u_t + H_\varepsilon(x, u_x) = 0. \tag{2.4}$$

We consider two cases of the Hamiltonian H_ε, where the kinetic coefficient $m(p) = p\tanh(\frac{1}{p})$ is suggested by [8, 9, 10]. Namely, we study

$$(i) \quad H^1_\varepsilon(x,p) = -m(\tfrac{p}{\varepsilon})\sqrt{1+p^2}\,\sigma(x), \quad (ii) \quad H^2_\varepsilon(x,p) = -m(\tfrac{p}{\varepsilon})\,\sigma(x)\,,$$

where the superscript of H is a mark to distinguish between *(i)* and *(ii)*. The parameter ε appearing in the last example is the criterion of the local slope. In our numerical study, we use the following equation for $\sigma(x)$,

$$\sigma(x) = \sigma_0(1-x^2)_+, \quad \sigma_0 > 0, \tag{2.5}$$

where the length is scaled by L and subscript of $+$ denotes the positive part.

The theoretical analysis of (2.4) augmented with the boundary (2.2) and initial conditions (2.3) is performed in Sections 3 and 4. In Section 5 we solve numerically equation (2.4) from the point of view of both 1) the method of characteristics for (2.4) with a Hamilton-Jacobi system of ordinary differential equations and 2) the conservation equation of step flux for (2.4).

3 The microscopic time scale approximation

We consider the initial-boundary problem of the form,

$$u^\varepsilon_t + H_\varepsilon(x, u^\varepsilon_x) = 0, \quad x > 0, \quad t > 0, \tag{3.1}$$

$$u^\varepsilon(0,t) = ct,\ t > 0 \quad \text{and} \quad u^\varepsilon(x,0) = 0,\ x > 0 \tag{3.2}$$

with $H_\varepsilon = H^1_\varepsilon$ given by (i), m as above and c is a given positive constant smaller than $\sigma_0 = \sigma(0)$. In this and next Sections we shall not make any reference to this particular definition of, but we will use that $c < \sigma(0)$.

We approximate the solution u^ε of (3.1)–(3.2) by introducing a new time variable (the fast time variable or the *microscopic time variable*) $\tau = t/\varepsilon$ so that

$$u^\varepsilon(x, \varepsilon\tau) = \varepsilon v(x, \tau) + o(\varepsilon) \text{ as } \varepsilon \to 0.$$

By replacing τ by t, we see that formally v solves

$$v_t + H(x, v_x) = 0, \tag{3.3}$$
$$v(0, t) = ct \ , \ v(x, 0) = 0 \tag{3.4}$$

with

$$H(x, p) = -m(p)\sigma(x) \equiv H^2_{\varepsilon=1}.$$

We call system (3.3)–(3.4) the *microscopic time scale approximation* of (3.1)–(3.2). Below, we will present a rigorous argument why (3.3)–(3.4) is indeed an approximation to (3.1)–(3.2). In the next section we shall see that both problems (3.1)–(3.2) and (3.3)–(3.4) admit a C^1 solution which is a unique viscosity solution, so we simply say it is a solution. The reader is referred to [17] and [18] for a general theory of viscosity solutions.

Theorem 3.1 *Let u^ε be the solution of (3.1)–(3.2) and v be the solution of the microscopic time approximation i.e. (3.3)–(3.4). We assume that σ is a nonnegative decreasing Lipschitz continuous function and $0 < c < \sigma_0 = \sigma(0)$. Then,*

$$v^\varepsilon(x, t) = \varepsilon^{-1} u^\varepsilon(x, \varepsilon t)$$

converges to v uniformly on every compact set of $[0, \infty) \times [0, \infty)$.

Sketch of the proof. A direct computation shows that v^ε satisfies

$$v_t + \overline{H}_\varepsilon(x, v_x) = 0 \ , \ v(0, t) = ct \ , \ v(x, 0) = 0 \tag{3.5}$$

with $\overline{H}_\varepsilon(x, p) = -m(p)\sigma(x)\sqrt{1 + (\varepsilon p)^2}$. We shall construct sub- and supersolutions of (3.5), which are independent from ε.

It is easy to notice that

$$v^+(x, t) = ct$$

is a supersolution of (3.5) satisfying the initial and boundary conditions. It is clear that $v_0 \equiv 0$ is a subsolution but the boundary condition is not fulfilled. Since we have assumed that $c < \sigma_0 = \sigma(0)$, there is a unique negative value p_0 such that $m(p_0) = c/\sigma_0$. We set

$$v_1(x, t) = ct\sigma(x)/\sigma_0 + p_0 x$$

and observe that v_1 is a subsolution of (3.5) satisfying the boundary condition but not the initial condition. Indeed,

$$v_{1t} + \overline{H}_\varepsilon(x, v_{1x}) = c\sigma(x)/\sigma_0 + \overline{H}_\varepsilon(x, ct\sigma'(x)/\sigma_0 + p_0) \le c\sigma(x)/\sigma_0 + H(x, p_0) = 0$$

because of monotonicity of m, as well as of positivity of m and σ. We now set

$$v^-(x, t) = \max(v_0, v_1) = \max(0, ct\sigma(x)/\sigma_0 + p_0 x)$$

and observe that v^- is a viscosity subsolution of (3.5) satisfying the initial and boundary conditions. At the same time we recall that the supremum of a family of viscosity subsolutions is again a viscosity subsolution [18, Lemma 2.4.1].

By a simple comparison theorem (see eg. [17, Theorem 3.3]) of viscosity solutions of evolution equations, we observe that

$$v^- \leq v^\varepsilon \leq v^+ \text{ in } [0,\infty) \times [0,\infty).$$

If one takes a relaxed limit

$$\overline{v} = \limsup{}^* v^\varepsilon \ , \ \underline{v} = \liminf_* v^\varepsilon,$$

we observe that $\overline{v}$ is a viscosity subsolution and that $\underline{v}$ is a viscosity supersolution. This is so by stability results, *e.g.,* [18, Theorem 2.2.1], because $\overline{H}_\varepsilon \to H$ as $\varepsilon \to 0$. The estimate by $v^\pm$ yields that $v^- \leq \underline{v} \leq \overline{v} \leq v^+$.

By the comparison theorem, we see that $\overline{v} \leq \underline{v}$ which yields $\underline{v} = \overline{v} (:= v)$. This function is a unique viscosity solution of (3.3)–(3.4). This property $\underline{v} = \overline{v}$ implies that v^ε converges to the unique viscosity solution of (3.3)–(3.4) locally uniformly in $[0,\infty) \times [0,\infty)$. (This technique to deduce convergence without estimating derivatives is due to Barles and Perthame [19], [20] and Ishii [21]; see also [18, Section 4.6]).

Remark 3.1 The convergence result, (Theorem 3.1), can be easily extended to deal with more general $\overline{H}^\varepsilon$ and H. For example, it is enough to assume that

$$\begin{array}{llll} (i) & \overline{H}_\varepsilon \leq H \leq 0, & (ii) & p \mapsto H(x,p) \text{ is nondecreasing} \\ (iii) & \overline{H}_\varepsilon(x,0) = 0, & (iv) & H(0,p) + c = 0 \text{ has a negative solution } p = p_0 \end{array}$$

to be able to construct a sub- and supersolution of (3.4) (independent of ε) satisfying the initial and boundary condition. Indeed, if we define v_1 as

$$v_1(x,t) = ctH(x,p_0) \ / \ H(0,p_0) + p_0 x,$$

then v^- and v^+ are still the desired sub- and supersolutions.

4 Explicit forms of solutions

We shall show that the method of characteristics gives an explicit form of solutions of both (3.1)–(3.2) and its microscopic time scale approximation (3.3)–(3.4). It turns out that at least near $x = 0$, the profile of the solution is independent of time. It is of the form $ct + b(x)$. Obviously, the substitution into the equation yields the relation $c + H(x,p) = 0$ for $p = b_x$. This leads to another important critical value x_c for H in (3.3) apart from x_e the smallest zero of σ; (we shall assume that $x_e = 1$ in order to simplify the notation). Namely, we set

$$x_c = \sup\{x > 0 |\ c + H(x,p) = 0 \text{ for some } p < 0\}. \tag{4.1}$$

We call the interval $(0, x_c)$, the *maximal stable region of a facet*. Since we have assumed $0 < c < \sigma_0 = \sigma(0)$, this region is non-empty. Moreover, $x_c < 1$ for H defined by (ii),

because by the definition of σ the supersaturation vanishes for $x \geq 1$. If instead, one defines x_c for H^1_ε, then it is clear that $x_c = 1$, because $m(p/\varepsilon)(1+p^2)^{1/2}$ is unbounded.

If $q(x)$ is the unique negative solution of $c + H(x, q) = 0$, then our explicit formula for a solution of (3.3) is as follows,

$$ct + b(x),$$

where $b(x) = \int_0^x q(\rho)d\rho$. This function is well-defined in $(0, x_c)$, however it does not satisfy the initial condition $(3.4)_2$. Thus, our convergence result, Theorem 3.1, says that the solution of (3.1)-(3.2) behaves like $ct + b(x)$ for large time.

Let us now look at the explicit formula from the view point of the theory of characteristics. We recall that a Hamilton-Jacobi system of ordinary differential equations for (3.3) is

$$\frac{dx}{dt} = H_p(x, p), \tag{4.2}$$

$$\frac{dp}{dt} = -H_x(x, p). \tag{4.3}$$

Since function H is constant along the characteristics, *i.e.*, on solution $(x(t), p(t))$ of (4.2)–(4.3), thus, by the definition of $q(x)$, we deduce that $p(t) = q(x(t))$ for $t \geq t_0$. Moreover, $c + H(0, p(t_0)) = 0$ for $t_0 \geq 0$ provided that $x(t_0) = 0$.

This implies that the function below

$$v(x, t) = ct + \int_0^x q(\rho)d\rho \qquad \text{for} \quad 0 < x < X_1(t),$$

is a solution of (3.3). Here $x = X_1(t)$ fulfills

$$\frac{dx}{dt} = H_p(x, q(x)), \qquad x(0) = 0. \tag{4.4}$$

We note that $X_1(t) \uparrow x_c$ as $t \to \infty$.

On the other hand, it is easy to describe the characteristic starting from $t = 0$, $x > 0$, because by (4.3) and the initial condition $(3.2)_2$ we have $p(0) = 0$. Thus, we conclude that $p(t) \equiv 0$. Hence, $x(t)$ is a solution of

$$\frac{dx}{dt} = H_p(x, 0)\ ,\ t > 0 \tag{4.5}$$

with $x(0) = x_0 \in (0, 1)$. It is clear that $x(t) \uparrow 1$ as $t \to \infty$, where $x = 1 = x_e$ is a unique equilibrium of the system for $x \leq 1$.

Now, we define $x = X_0(t)$ as a unique solution of (4.5) with $X_0(0) = 0$. Thus, the family of all solution (4.5) for $x(0) > 0$ sweeps all the region $X_0(t) < x < 1$. Finally,

$$v(x, t) = 0 \qquad \text{for} \quad X_0(t) < x$$

since for $x \geq 1$ we have trivially $\sigma \equiv 0$ and as a result $v \equiv 0$.

Interestingly, there is a gap between $X_1(t)$ and $X_0(t)$ *i.e.*, $X_1(t) < X_0(t)$ for $t > 0$. This region corresponds to the rarefaction region. It is covered by a monotone family of $x = x(t, r)$ with respect to $r \in (q(0), 0)$, where $x = x(t, r)$ solves (4.2)–(4.3), with $x(0) = 0$, $p(0) = r$. The value $v(x(t, r), t)$ is implicitly determined by

$$\frac{dv}{dt} = -H(x(t), p(t)) + p(t)H_p(x(t), p(t)), \quad v(0) = 0.$$

By the continuous dependence of initial data, we see that the slope of v is continuous in x and t so this gives a unique C^1 solution of (3.3)–(3.4). The same argument applies to (3.1)–(3.2), even in the case $x_c = 1$.

We summarize what we obtained.

Theorem 4.1 *Assume that $\sigma(x)$ is a nonnegative decreasing Lipschitz continuous function which is smooth, except possibly the point $x_e = 1$. The unique C^1 solution v of (3.3)–(3.4) with $H = H^2_{\varepsilon=1}$ is of the form*

$$\begin{aligned} &v(x,t) = ct + \int_0^x q(p)\,dp\,, && \text{for } 0 < x < X_1(t)\,, \\ &v(x,t) = 0\,, && \text{for } X_0(t) \le x\,, \end{aligned}$$

where X_1 is a solution of (4.4) and X_0 solves (4.5) with $X_0(0) = 0$. The function $X_1(t) \uparrow x_c$ and $X_0(t) \uparrow 1$ as $t \to \infty$. Moreover, $X_1(t) < X_0(t)$ for $t > 0$.

Remark 4.1 If $c \ge \sigma(0)$, then the whole region $0 < x < X_0(t)$ is the rarefaction region for (3.3)–(3.4). The solution constructed by the method of characteristic does not achieve the boundary condition in classical sense. However, it is still a viscosity solution of (3.3)–(3.4).

Remark 4.2 Our results now give a clear view of the solution of (3.1)–(3.2) with small ε. By Theorem 3.1 and Theorem 4.1 we have

$$\begin{aligned} u(x,t) &= \varepsilon v(x, t/\varepsilon) + o(\varepsilon) \\ &= \varepsilon(ct/\varepsilon + b(x)) + o(\varepsilon) \\ &= ct + \varepsilon b(x) + o(\varepsilon)\,, \end{aligned}$$

for $x \in (0, X_1(t/\varepsilon))$ as $\varepsilon \to 0$ for $t = O(\varepsilon)$ where

$$b(x) = \int_0^x q(p)dp\,.$$

Roughly speaking, $u(x,t)$ is flat up to order ε in the region $(0, x_c)$. Outside this region u, cannot attain the speed c.

We note here that, if we have a solution to (2.4) in the form given by the above Theorem, *i.e.*,

$$u(x,t) = V_0 t + b(x)\,,$$

then we can have

$$V_0 = m(b_x)\sqrt{1 + b_x^2}\,\sigma(x)\,,$$

where b_x is a local slope. When $b_x \ll 1$, this expression is the same criterion of stable growth of polyhedral crystal as that of Chernov [7],

$$V_0 = m(g_x)\,\sigma(x)\,.$$

We emphasize that this equation is only valid in the region $0 \le x < x_c$, where x_c is a critical length to be determined by (4.1).

5 Numerical results

In this section, we solve numerically equation (2.4) having the form of supersaturation (2.5) under the conditions of (2.2) and (2.3). In our calculations we take c as in (2.2). For simplicity, we take the ratio of ε to σ_0 equal to one, so that $c/\sigma_0 = \tanh(1)$.

5.1 Method of characteristics for a Hamilton-Jacobi system

The characteristic curves in the (x, t)-plane for the Hamilton-Jacobi system for (2.4) are numerically obtained by the ordinary differential equations (4.2) and (4.3) as shown in Figures 1, 2, 3 and 4 for four different values of $\sigma_0 = \varepsilon = 1.0$, 0.1, 0.01 and 0.001, respectively. Figures 1(a), 2(a), 3(a) and 4(a) correspond to the case *(i)* of the Hamiltonian, while simulation for the microscopic time approximation (*i.e.*, the case of *(ii)*) are shown in Figures 1(b), 2(b), 3(b) and 4(b). The characteristic curves starting from the ordinate axis, $x = 0$, are obtained by solving simultaneously both (4.2) and (4.3) using the forth-order Runge-Kutta method [22] and are plotted with solid curves at equal intervals of time beginning with $t = 0$.

Figures 1, 2, 3 and 4, except Figure 3(c), also show the characteristic curves plotted in dashed lines with local slope $p = 0$ from the abscissa axis, $t = 0$, at equal intervals of space beginning with $x = 0.1$, and the characteristic curve plotted in dash-dotted lines starting from the origin has a constant local slope p given by $c + H^1_\varepsilon(0, p) = 0$ in Figures 1(a), 2(a), 3(a) and 4(a), and p given by $c + H^2_\varepsilon(0, p) = 0$, *i.e.*, $p = \sigma_0$ in Figures 1(b), 2(b), 3(b) and 4(b). As time increases, these characteristic curves approach $x = 1$, where $\sigma(1) = 0$. All figures, except Figure 1(a), display the rarefaction region between the characteristic curve from the origin and the characteristic curves from the ordinate axis $x = 0$, as mentioned just before Theorem 4.1. The rarefaction region is not visible in Figure 1(a).

We will discuss the differences visible on the plots for various values of parameters. On first picture the simulations for $\varepsilon = 1.0$ and $\sigma_0 = 1.0$ are presented. The plot on Figure 1(b) clearly indicates that the characteristic curves emanating from the line $x = 0$ converge to the critical point x_c, while Figure 1(a) shows that the characteristic curves starting at $x = 0$ approach $x = 1$ as time progresses. Figure 2 presents the results for $\varepsilon = 0.1$ and $\sigma_0 = 0.1$. Despite of the similarity between Figure 1(b) and Figure 2(b) showing convergence to the critical point x_c of the characteristic curves beginning at $x = 0$, there is a pronounced difference between the calculations for $\varepsilon = 1.0 = \sigma_0$ and $\varepsilon = 0.1 = \sigma_0$. Namely, Figure 2(a) shows that the characteristics bend around x_c and they are expected to approach $x = 1$ after long time.

The characteristic curves for $\varepsilon = 0.01$ and $\sigma_0 = 0.01$ are drawn on Figure 3. Its part (a), compared to Figure 2(a), suggests that the curves emanating from the axis $x = 0$ converge to x_c as time develops. However even in this case, x_c is not a stationary point. This statement is supported by Figure 3(c), showing that the characteristic curves go beyond x_c and the propagation lasts ten times longer time than in Figure 2(a). This is why the point x_c in Figure 3(a) is *a metastable point*. Figure 3(b) also clearly shows that the characteristics curves starting from $x = 0$ converge to the critical point x_c, this is in accordance with Figure 1(b).

Since the solution u^ε of *(ii)* for general $\varepsilon = \sigma_0$ is obtained by a simple scaling of the solution w of *(ii)* with $\varepsilon = 1$ by $u^\varepsilon(x, t) = \varepsilon w(x, t)$, the behavior of convergence is independent of ε. Figure 4 shows the characteristic curves for $\varepsilon = 0.001$ and $\sigma_0 = 0.001$. When ε decreases, the characteristic curves starting from $x = 0$ appear to be closer to x_c

than in the case of large ε, as shown in Figure 4(a). This tendency is consistent with the microscopic time scale approximation, discussed in Section 3. The characteristics curves, starting from $x = 0$ in Figure 4(b), also converge to the critical point x_c, in the same way as in Figure1(b).

5.2 Conservation equation of step flux

The equation of (2.4) has the form of a conservation of step flux equation:

$$u_t = S_\varepsilon(x, u_x)\,, \tag{5.1}$$

where $S_\varepsilon(x, u_x)$ is

$$(i)\quad S^1_\varepsilon(x, u_x) = \tfrac{1}{\varepsilon}\tanh(\tfrac{\varepsilon}{u_x})\sqrt{1+u_x^2}\,\sigma(x), \quad (ii)\quad S^2_\varepsilon(x, u_x) = \tfrac{1}{\varepsilon}\tanh(\tfrac{\varepsilon}{u_x})\,\sigma(x)\,,$$

where the superscript of S corresponds to the case of *(i)* or *(ii)*. We solve numerically equation (5.1) augmented with the boundary condition (2.2) and the initial condition (2.3) for the supersaturation having the form (2.5). For this purpose we use the upwind differencing scheme, see [22].

Our numerical results, for the same conditions as in Figures 1, 2, 3 and 4, are shown in Figures 5, 6, 7 and 8, respectively. All top figures represent the graph of the growth rates V as a function of x at various time t. All bottom figures represent the profiles of crystal, *i.e.*, the height $z = u(x, t)$ scaled by σ_0. The results in the case of *(i)* are shown in Figures 5(a), 6(a) 7(a) and 8(a), while for the microscopic time approximation, *i.e.*, in the case of *(ii)*, are shown in Figures 5(b), 6(b), 7(b) and 8(b).

Numerical results, as shown in Figures 5(b), 6(b), 7(b) and 8(b), demonstrate *the maximal stable region of a facet* as mentioned in Section 4, where the stable region is not perfectly flat but changes according to the term $\int_0^x q(p)\,dp$ as in Theorem 4.1. When the number of figure increases from 5 to 7, *i.e.*, ε decreases, the results (a) are closer to (b) as shown in Figures 5, 6 and 7. In other words the case *(i)* get closer to the case *(ii)* with decreasing ε. Finally we notice that, we can not distinguish between Figures 8 (a) and 8 (b). As mentioned in Remark 4.2, the facet in the region (0, x_c) is flat up the order of ε^1. All numerical results, as shown in Figures 5, 6, 7 and 8 are consistent both with the microscopic time scale approximation of Section 3 and with the numerical method of characteristics.

Acknowledgment. The research for this paper was initiated when the first author was a guest professor of the University of Tokyo and the third author visited the univerisity. Both thank the university for its hospitality. The work of Y.G. was in part supported by the Gran-in-Aid for Scientific Research, No.18204011, No.17654037, the Japan Society of the Promotion of Science (JSPS). The work of P.R. was in part supported by Polish KBN grant No.1 P03A 037 28.

References

[1] W. K. Burton, N. Cabrera and F. C. Frank, The growth of crystals and the equilibrium structure of their surfaces, *Phil. Trans. Roy. Soc. London A*, **243**, (1951), 299–358.

[2] W. E, N.K. Yip, Continuum Theory of Epitaxial Crystal Growth. I *J. Statistical Physics*, **104**, (2001), 221–253.

[3] R.V. Kohn, T.S. Lo and N.K. Yip, Continuum Limit of a Step Flow Model of Epitaxial Growth *Mat. Res. Soc. Symp. Proc.,* **696**, (2002).

[4] T.S. Lo and R.V. Kohn, A new approach to the continuous modeling of epitaxial growth: slope selection, coarsening, and the role of the uphill current, *Physica D*, **161,** (2002), 237–257.

[5] T.P.Schulze, R.V.Kohn, A geometric model for coarsening during spiral-mode growth of thin films, *Physica D,* **132**, (1999), 520–542.

[6] A. A. Chernov, Application of the method of characteristics to the theory of the growth forms of crystals, *Soviet Physics – Crystallography*, **8**, (1964), 401–405.

[7] A. A. Chernov, Stability of faceted shapes, *J. Crystal Growth*, **24/25**, (1974) 11-31.

[8] T. Kuroda, T. Irisawa and A. Ookawa, Growth of a polyhedral crystal from solution and its morphological stability. *J. Crystal Growth*, **42** , (1977), 41–46.

[9] E. Yokoyama and T. Kuroda, Pattern formation in growth of snow crystals occurring in the surface kinetic process and the diffusion process. *Physical Review A*, **41**, (1990) 2038–2049

[10] E. Yokoyama, Formation of patterns during growth of snow crystals, *J. Crystal Growth,* **128**, (1993) 251–257.

[11] E. Yokoyama and T. Kuroda, Quantitative investigation of rate determining process of growth of snow crystals– two-dimensional nucleation growth and spiral growth *J. Meteor. Soc. Japan*, **66**, (1988), 927–936.

[12] W. F. Berg, Crystal growth from solutions, *Proc. Roy. Soc., A.* **164**, (1938), 79–95.

[13] A. Seeger, Diffusion problems associated with the growth of crystals from dilute solution, *Phil. Mag.* **44**, (1953),1–13.

[14] H.Ishii, Asymptotic solutions for large time of Hamilton-Jacobi equations in Euclidean n space, *preprint*.

[15] H.Ishii, Asymptotic solutions for large time of Hamilton-Jacobi equations, Vol. III, 213-227. Eur. Math. Soc., Zurich (2006).

[16] Y. Giga, P. Rybka, Stability of facets of crystals growing from vapor, *Discrete Contin. Dyn. Syst.*, **14**, (2006), 689–706.

[17] M. G. Crandall, H. Ishii and P.-L. Lions, User's guide to viscosity solutions of second order partial differential equations, *Bull. Amer. Math. Soc.*, **27**, (1992), 1-67.

[18] Y. Giga, Surface evolution equations - A level set approach, *Monographs in Mathematics, 99, Birkhauser Verlag, Basel-Boston-Berlin*, (2006).

[19] G. Barles and B. Perthame, Discontinuous solutions of deterministic optimal stopping time problems, *RAIRO Model. Math. Anal. Numer.*, **21**, (1987), 557-579.

[20] G. Barles, and B. Perthame, Exit time problems in optimal control and vanishing viscosity method, *SIAM J. Control Optim.*, **26**, (1988), 1133-1148.

[21] H. Ishii, A boundary value problem of the Dirichlet type for Hamilton-Jacobi equations, *Ann. Scuola Norm. Sup. Pisa Cl. Sci. (4)*, **16**, (1989), 105–135.

[22] W. H. Press, S. A. Teukolsky, W. T. Vetterling and B. P. Flannery, *Numerical Recipes in C the Art of Scientific Computing Second Edition*, Cambridge University Press, (1992).

Figure Captions

Figure 1 The characteristic curves in (x, t) plane for a Hamilton-Jacobi system (2.4), $\sigma(x)$ = $\sigma(0)(1-x^2)_+$, σ_0 =1, ε = 1 and c = $\tanh(1)\sigma_0$; the solid curves are obtained by the ordinary differential equations (4.2) and (4.3); the dashed curves have a constant local slope for p = 0 starting from t =0; the dash-dotted curve starting from the origin has a constant local slope p given by $c + H^1_\varepsilon(0,p)$ = 0; the dotted line represents the critical point x_c; (a) corresponds to the case of *(i)* $H^1_\varepsilon(x,p) = -m(\frac{p}{\varepsilon})\sqrt{1+p^2}\,\sigma(x)$. (b) corresponds to the case of *(ii)* $H^2_\varepsilon(x,p) = -m(\frac{p}{\varepsilon})\,\sigma(x)$; the dash-dotted curve starting from the origin has a constant local slope p given by $c + H^2_\varepsilon(0,p)$ = 0, *i.e.*, p = σ_0. A rarefaction region develops between the dash-dotted curve and the solid curves.

Figure 2 The characteristic curves in (x, t)-plane for $\sigma_0 = 0.1$, $\varepsilon = 0.1$ and $c = \tanh(1)\sigma_0$; all curves are represented as in Figure 1. A rarefaction region develops between the dash-dotted curve and the solid curves.

Figure 3 The characteristic curves in $(x,\ t)$-plane for $\sigma_0 = 0.01$, $\varepsilon = 0.01$ and $c = \tanh(1)\sigma_0$; all curves are represented as in Figure 1. A rarefaction region develops between the dash-dotted curve and the solid curves. (c) the characteristic curves propagate ten times slower than in (a).

Figure 4 The characteristic curves in $(x,\ t)$-plane for $\sigma_0 = 0.001$, $\varepsilon = 0.001$ and $c = \tanh(1)\sigma_0$; all curves are represented as in Figure 1. A rarefaction region develops between the dash-dotted curve and the solid curves.

Figure 5 The growth rates V as a function of x at various time instances t in the top figure, and the profiles of crystal, *i.e.*, the height $z = u(x,t)$ scaled by σ_0 in the bottom for the same conditions as Figure 1, *i.e.*, $\sigma_0 = 1$, $\varepsilon = 1$ and $c = \tanh(1)\sigma_0$; (a) corresponds to the case of *(i)*, and (b) corresponds to the case of *(ii)*, *i.e.*, the microscopic time approximation.

Figure 6 The growth rates V as a function of x at various time instances t in the top figure, and the profiles of crystal, *i.e.*, the height $z = u(x,t)$, scaled by σ_0 in the bottom for the same conditions as Figure 2, *i.e.*, $\sigma_0 = 0.1$, $\varepsilon = 0.1$ and $c = \tanh(1)\sigma_0$; (a) corresponds to the case of *(i)*, and (b) corresponds to the case of *(ii)*.

Figure 7 The growth rates V as a function of x at various time instances t in the top figure, and the profiles of crystal, *i.e.*, the height $z = u(x,t)$ scaled by σ_0 in the bottom for the same conditions as Figure 3, *i.e.*, $\sigma_0 = 0.01$, $\varepsilon = 0.01$ and $c = \tanh(1)\sigma_0$; (a) corresponds to the case of *(i)*, and (b) corresponds to the case of *(ii)*.

Figure 8 The growth rates V as a function of x at various time instances t in the top figure, and the profiles of crystal, *i.e.*, the height $z = u(x,t)$ scaled by σ_0 in the bottom for the same conditions as for Figure 4, *i.e.*, $\sigma_0 = 0.001$, $\varepsilon = 0.001$ and $c = \tanh(1)\sigma_0$; (a) corresponds to the case of *(i)*, and (b) corresponds to the case of *(ii)*.

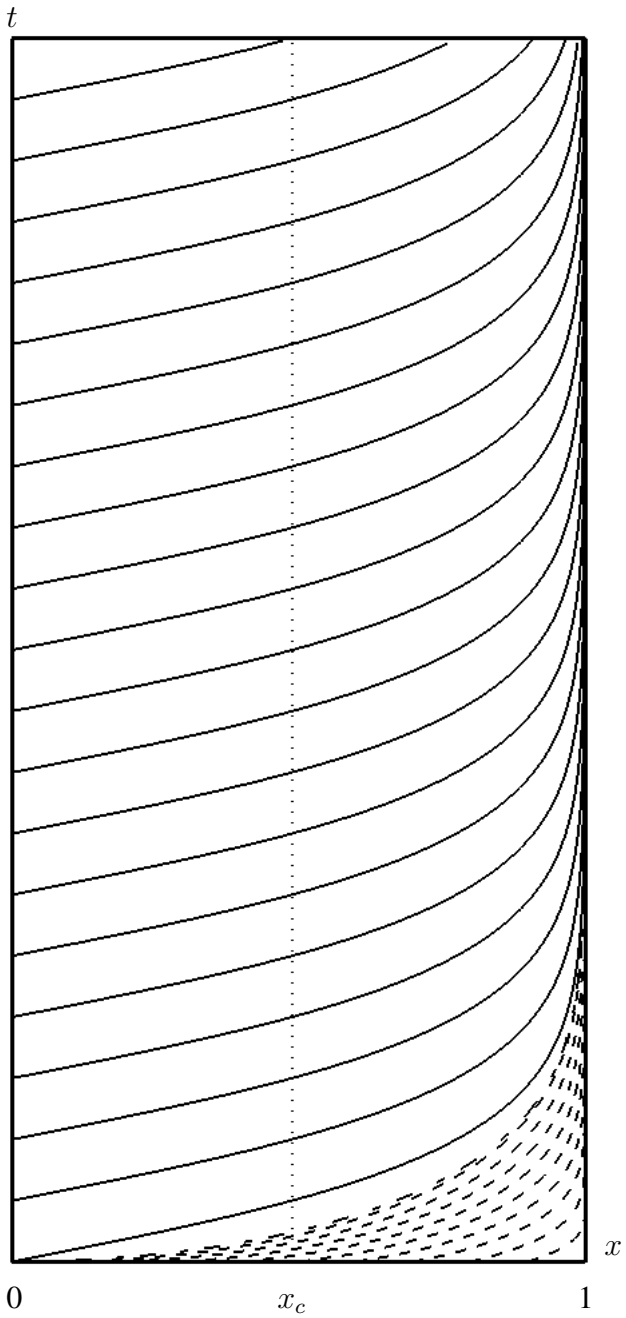

Figure 1: (a) The characteristic curves in (x, t) plane for a Hamilton-Jacobi system (2.4), $\sigma(x)$ = $\sigma(0)(1-x^2)_+$, σ_0 =1, ε = 1 and $c = \tanh(1)\sigma_0$; the solid curves are obtained by the ordinary differential equations (4.2) and (4.3); the dashed curves have a constant local slope for p = 0 starting from t =0; the dash-dotted curve starting from the origin has a constant local slope p given by $c + H^1_\varepsilon(0, p)$ = 0; the dotted line represents the critical point x_c; (a) corresponds to the case of *(i)* $H^1_\varepsilon(x, p) = -m(\frac{p}{\varepsilon})\sqrt{1+p^2}\,\sigma(x)$.

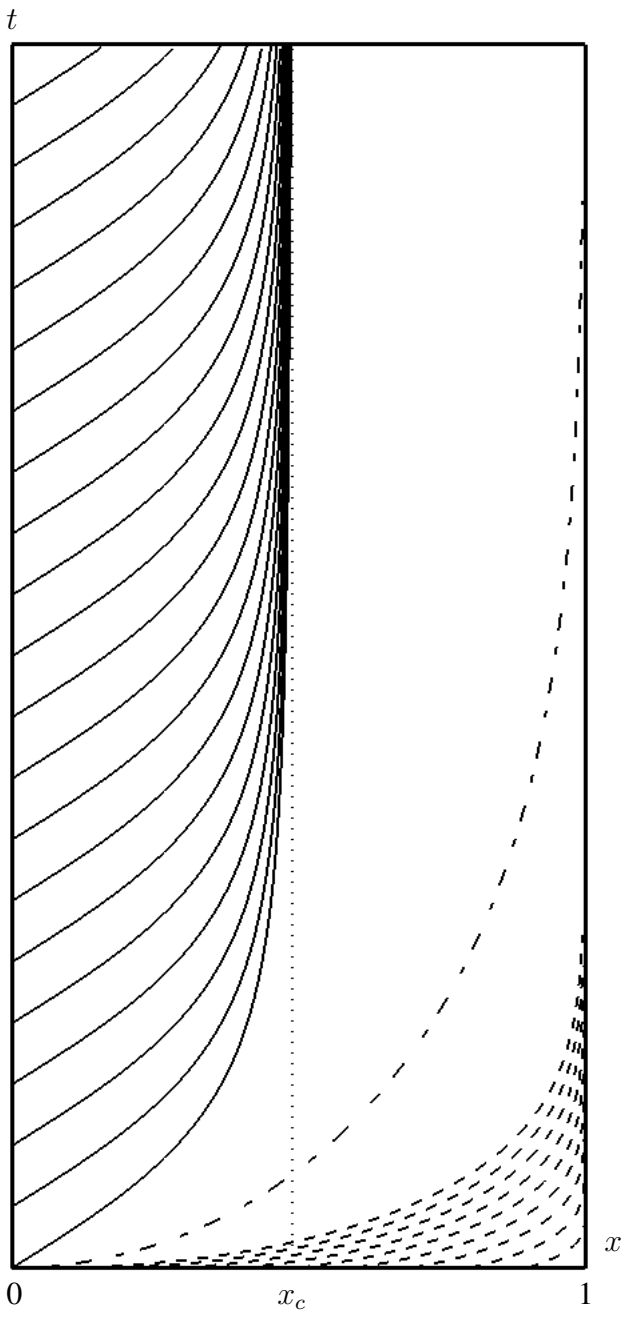

Figure 1: (b) the case of *(ii)* $H^2_\varepsilon(x,p) = -m(\frac{p}{\varepsilon})\,\sigma(x)$; the dash-dotted curve starting from the origin has a constant local slope p given by $c + H^2_\varepsilon(0,p) = 0$, *i.e.*, $p = \sigma_0$. A rarefaction region develops between the dash-dotted curve and the solid curves.

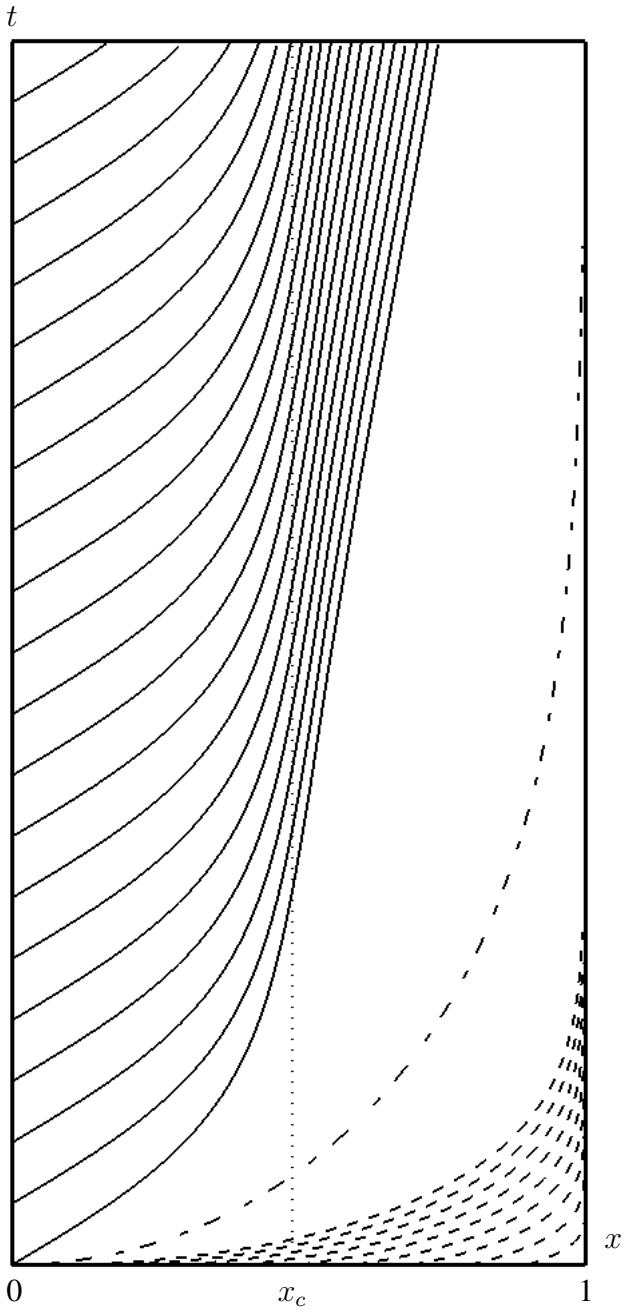

Figure 2: (a) The characteristic curves in $(x,\, t)$-plane for $\sigma_0 = 0.1$, $\varepsilon = 0.1$ and $c = \tanh(1)\sigma_0$; all curves are represented as in Figure 1. A rarefaction region develops between the dash-dotted curve and the solid curves.

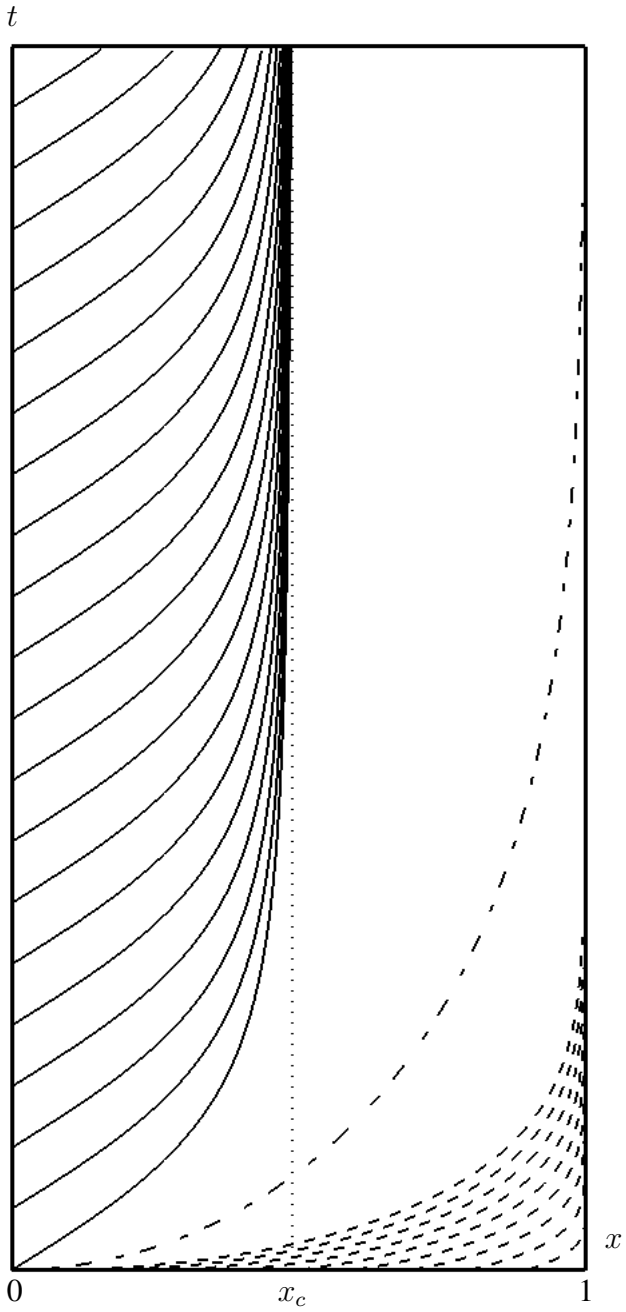

Figure 2: (b)

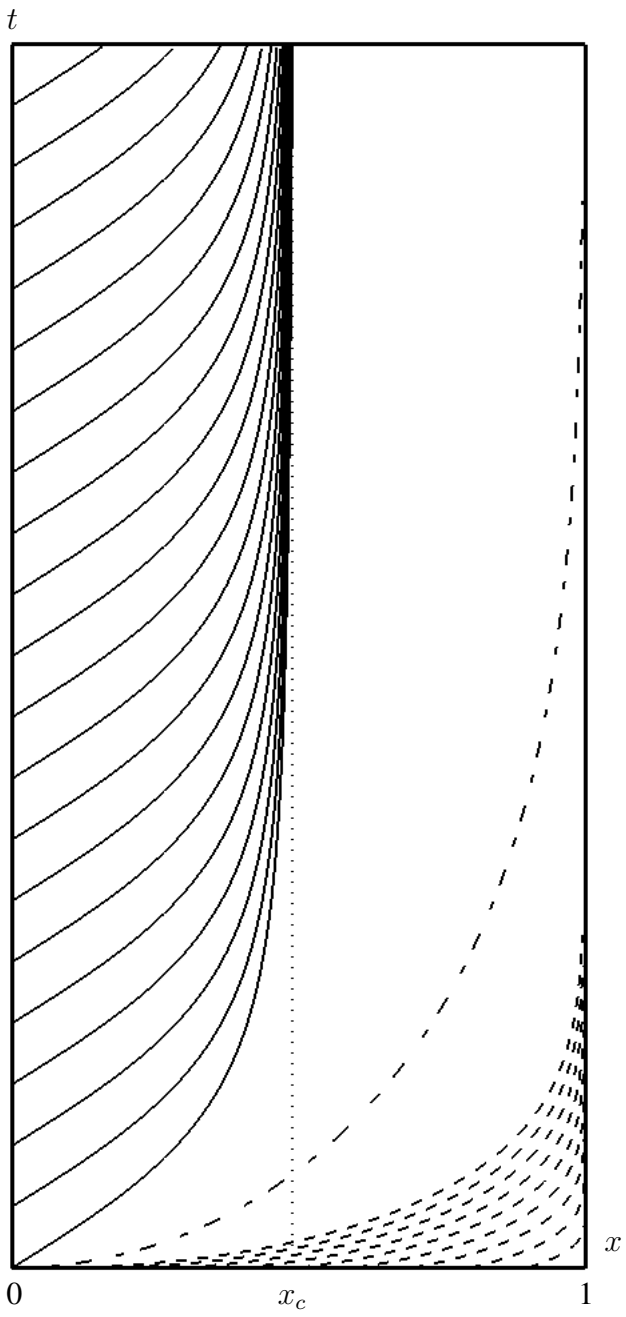

Figure 3: (a) The characteristic curves in $(x,\ t)$-plane for $\sigma_0 = 0.01$, $\varepsilon = 0.01$ and $c = \tanh(1)\sigma_0$; all curves are represented as in Figure 1; A rarefaction region develops between the dash-dotted curve and the solid curves.

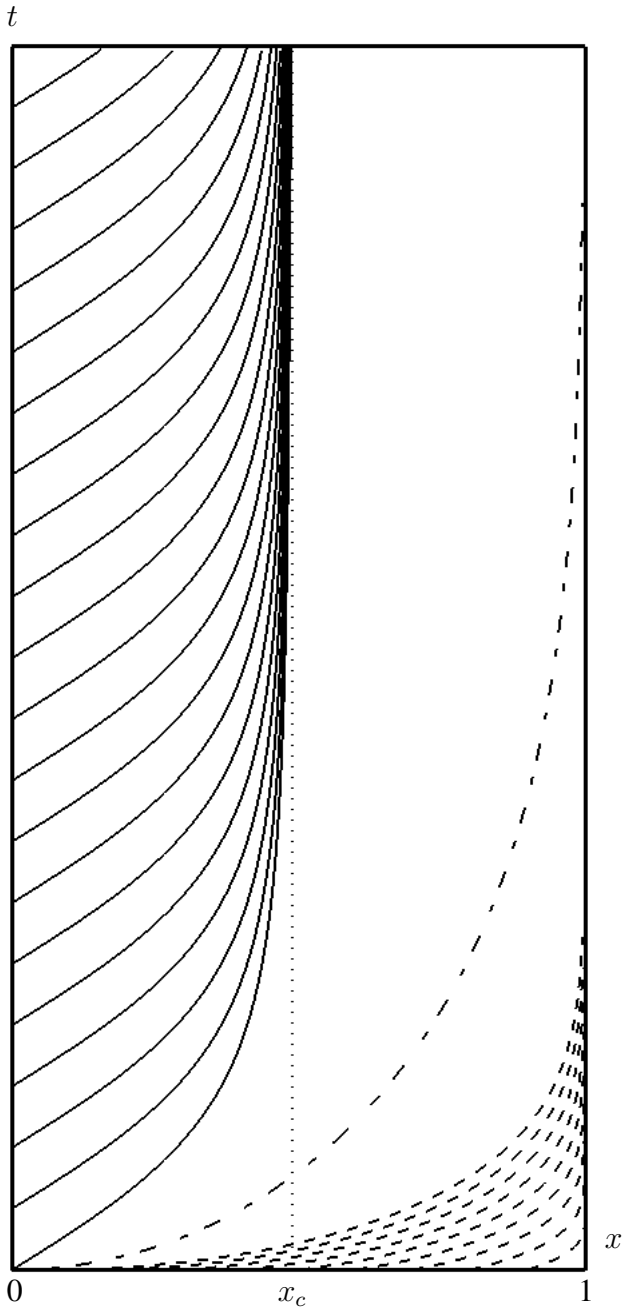

Figure 3: (b)

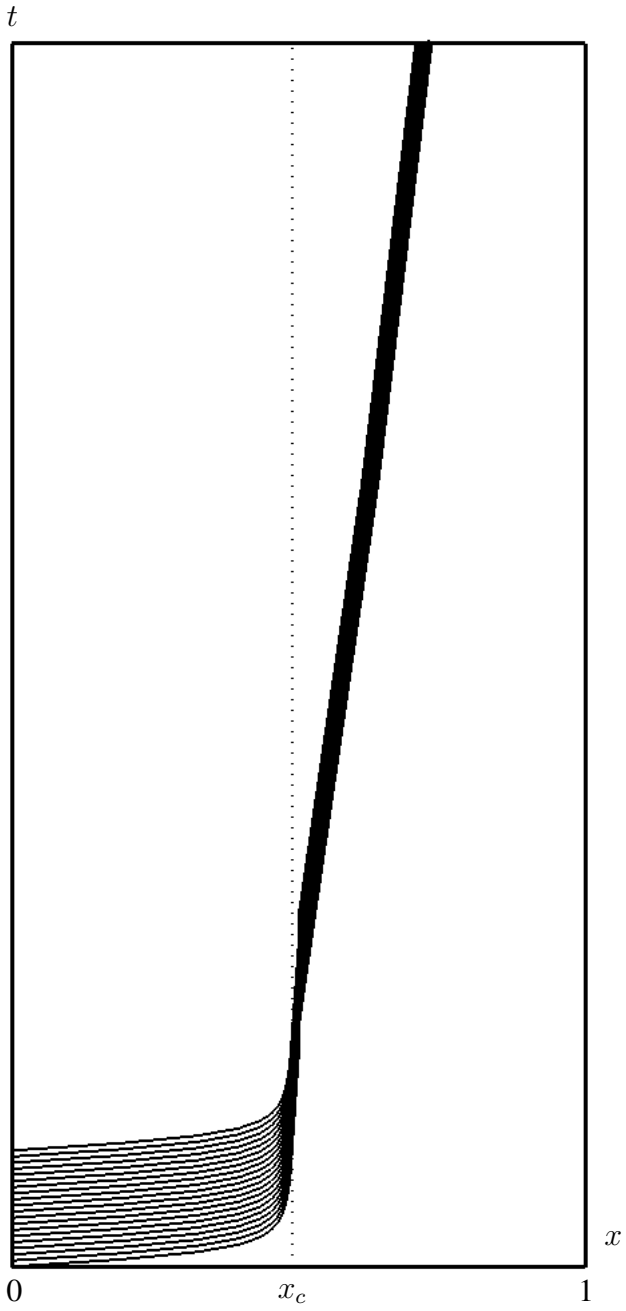

Figure 3: (c) the characteristic curves propagate ten times slower than in (a).

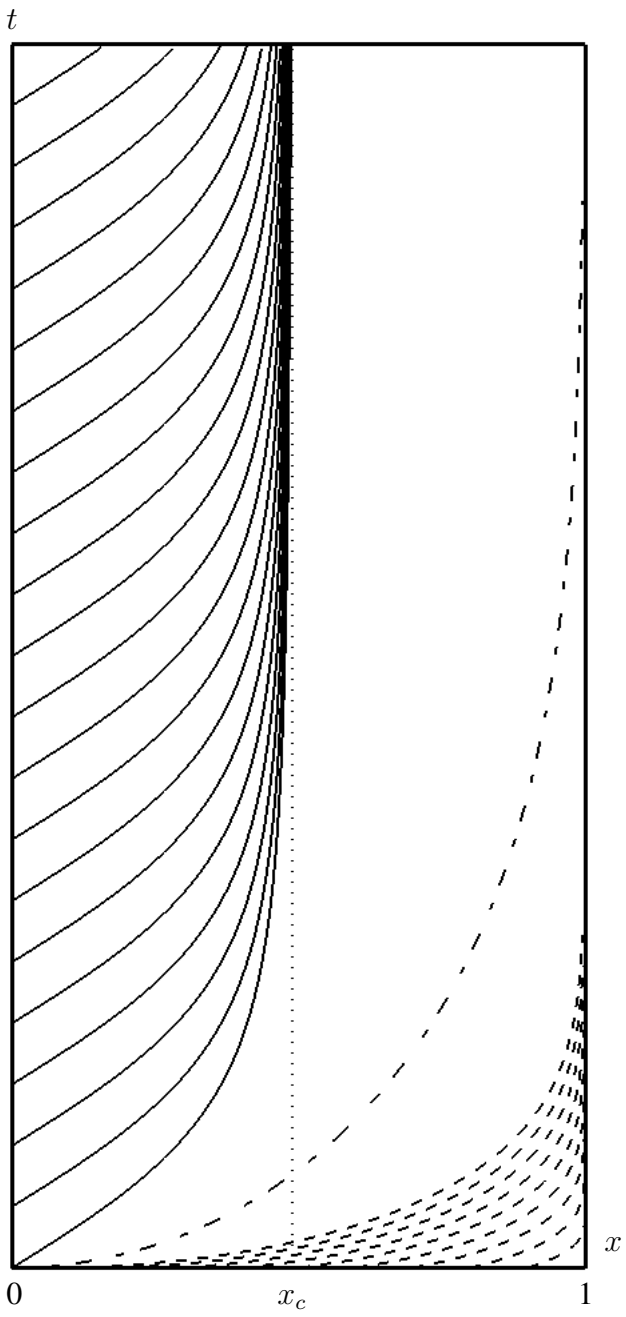

Figure 4: (a) The characteristic curves in (x, t)-plane for $\sigma_0 = 0.001$, $\varepsilon = 0.001$ and $c = \tanh(1)\sigma_0$; all curves are represented as in Figure 1. A rarefaction region develops between the dash-dotted curve and the solid curves.

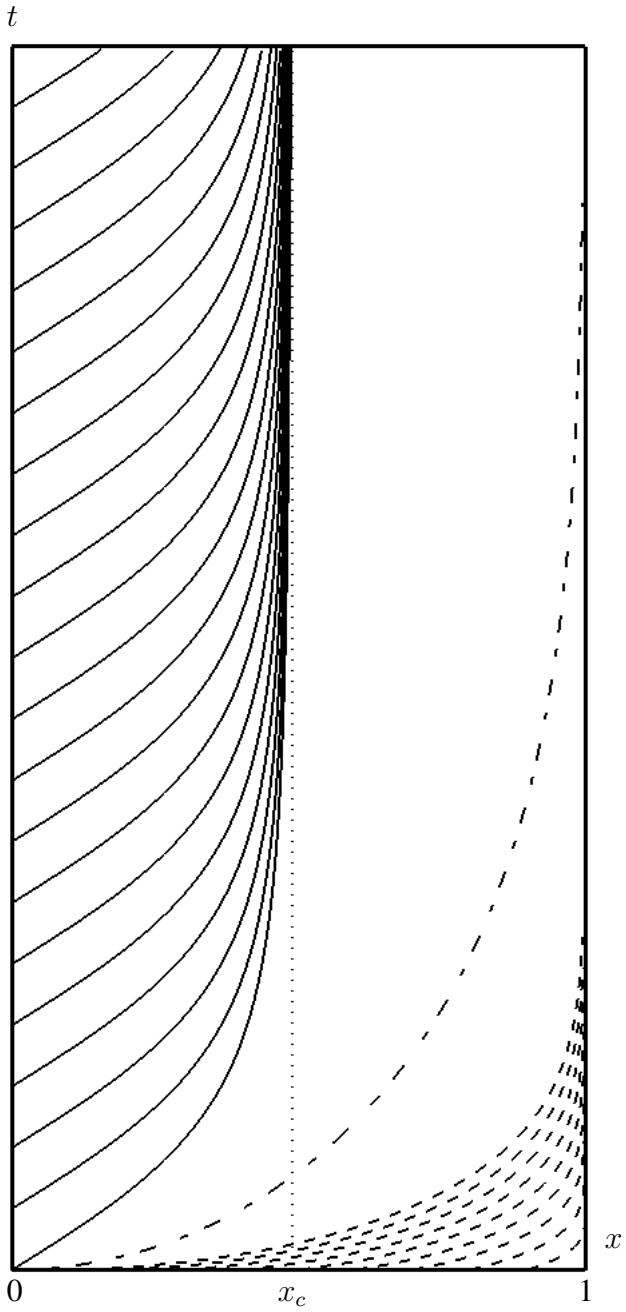

Figure 4: (b)

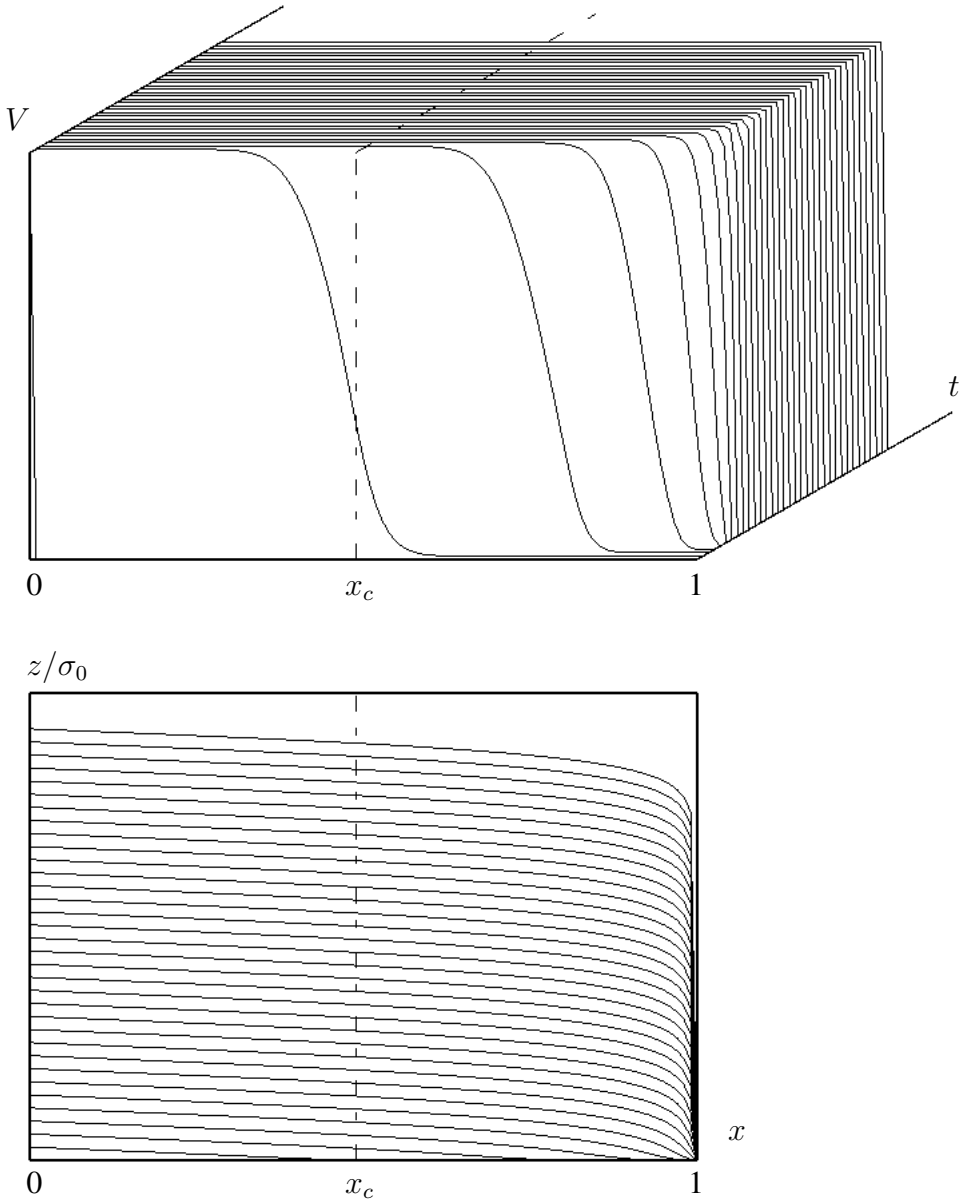

Figure 5: (a) The growth rates V as a function of x at various time instances t in the top figure, and the profiles of crystal, *i.e.*, the height $z = u(x, t)$ scaled by σ_0 in the bottom for the same conditions as Figure 1, *i.e.*, $\sigma_0 = 1$, $\varepsilon = 1$ and $c = \tanh(1)\sigma_0$; (a) corresponds to the case of *(i)*, and

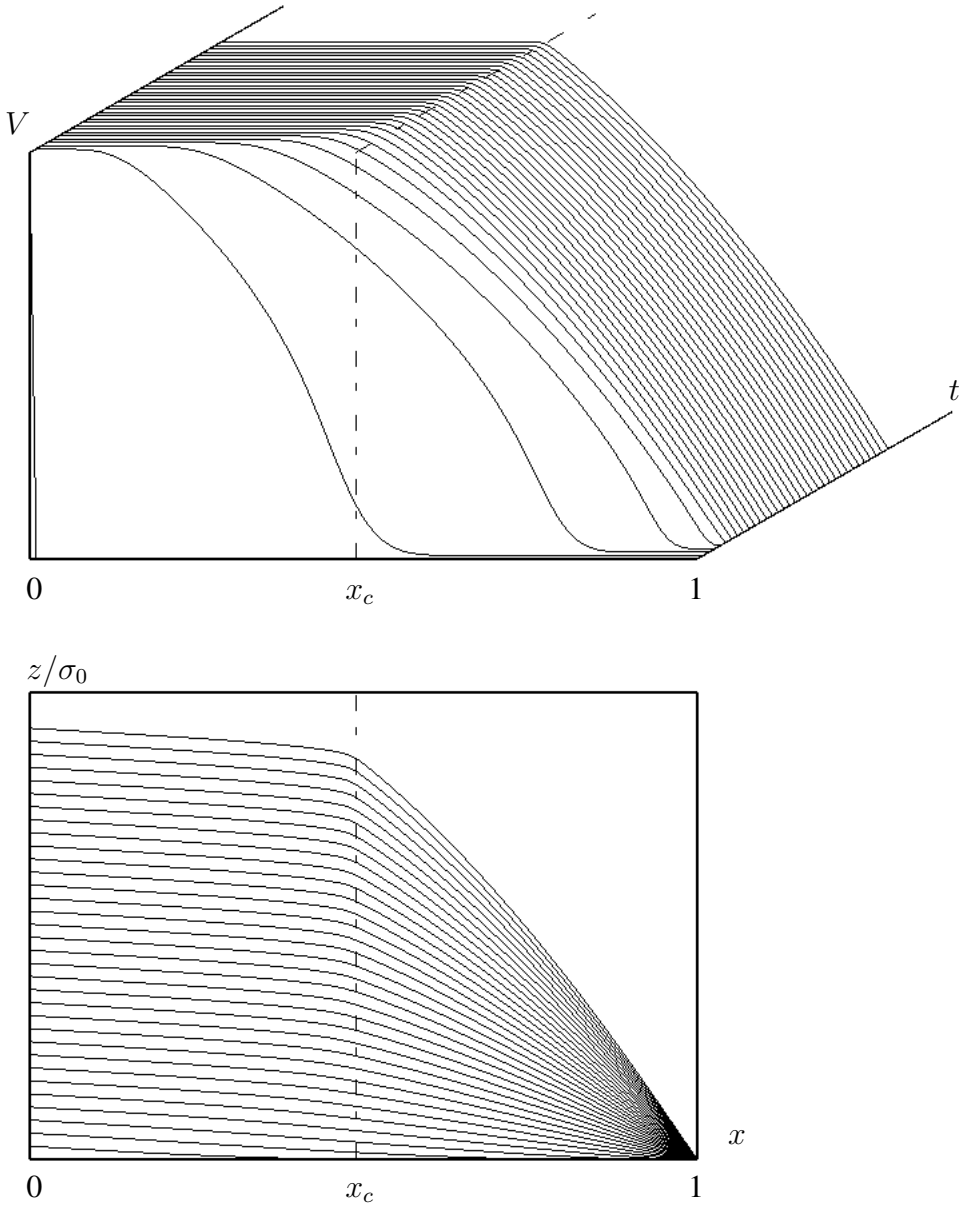

Figure 5: (b) corresponds to the case of *(ii)*, *i.e.*, the microscopic time approximation.

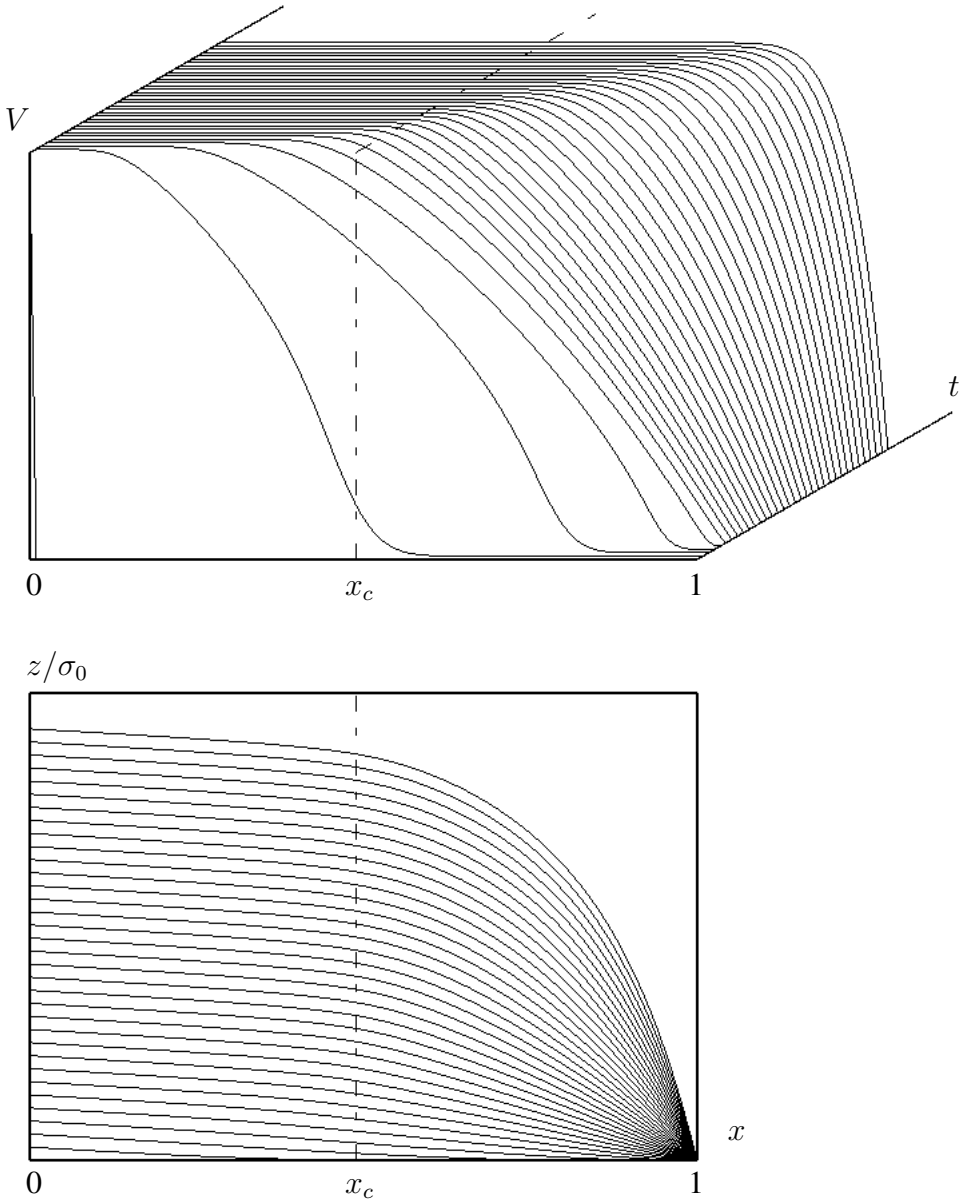

Figure 6: (a) The growth rates V as a function of x at various time instances t in the top figure, and the profiles of crystal, *i.e.*, the height $z = u(x, t)$, scaled by σ_0 in the bottom for the same conditions as Figure 2, *i.e.*, $\sigma_0 = 0.1$, $\varepsilon = 0.1$ and $c = \tanh(1)\sigma_0$; (a) corresponds to the case of *(i)*, and

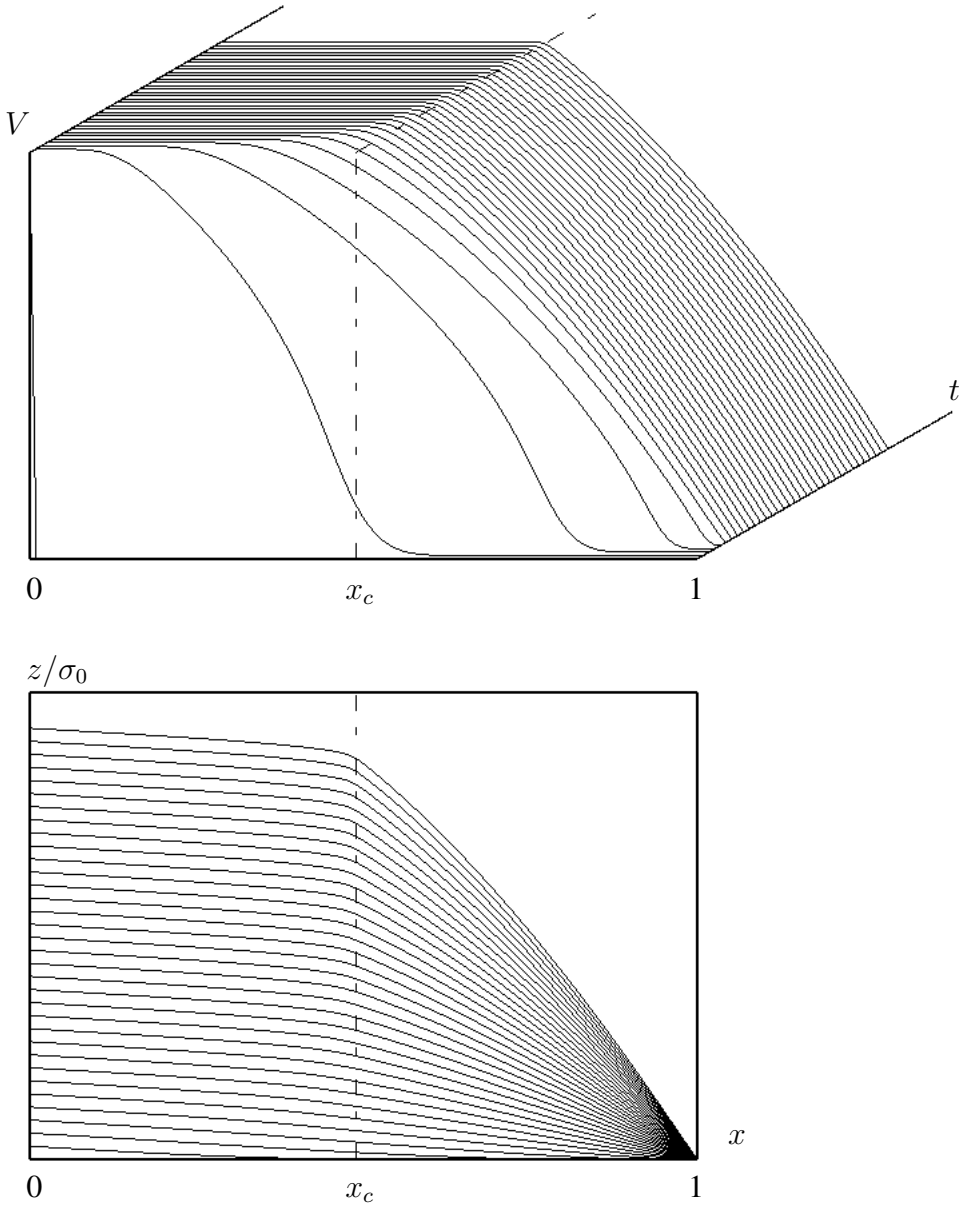

Figure 6: (b) corresponds to the case of *(ii)*.

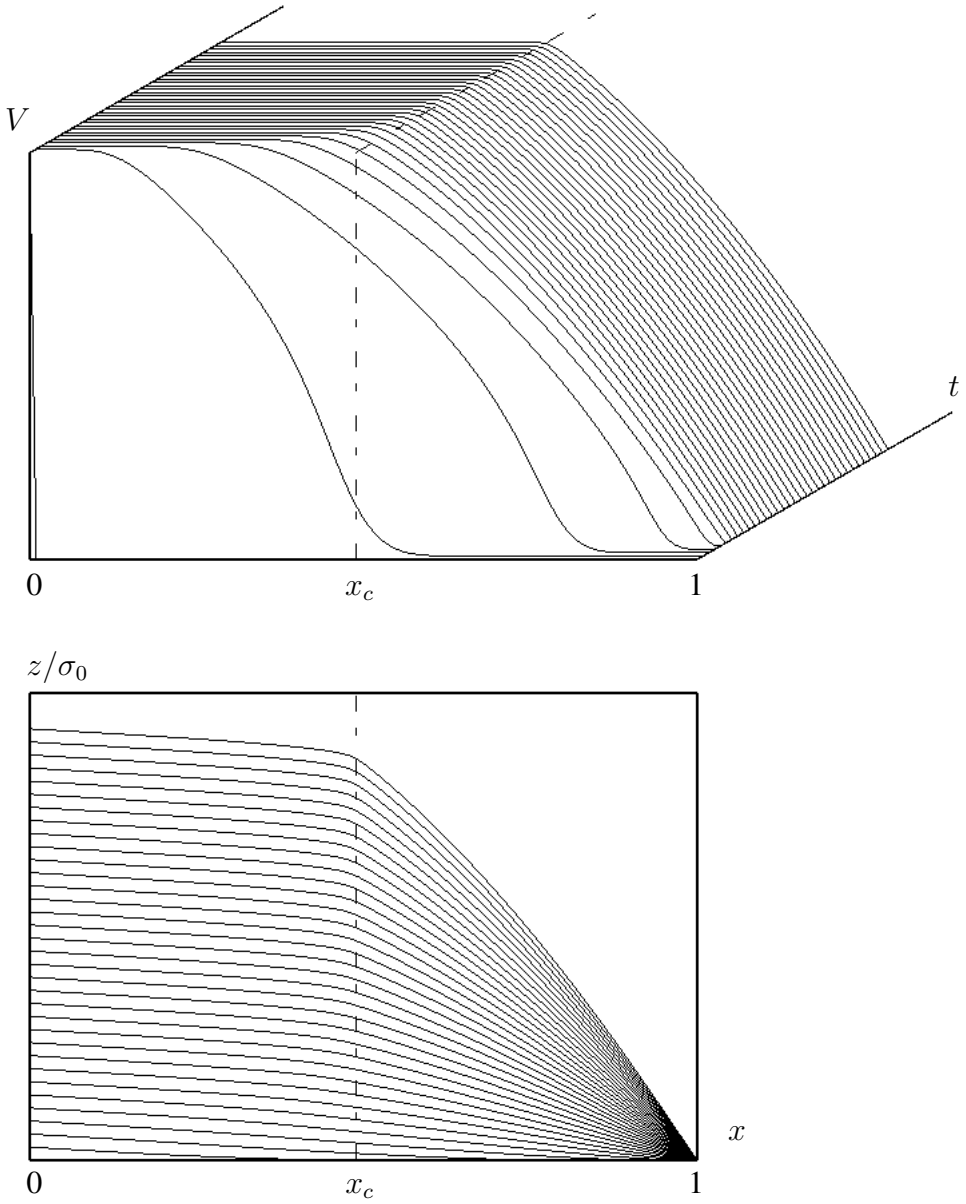

Figure 7: (a) The growth rates V as a function of x at various time instances t in the top figure, and the profiles of crystal, *i.e.*, the height $z = u(x,t)$ scaled by σ_0 in the bottom for the same conditions as Figure 3, *i.e.*, $\sigma_0 = 0.01$, $\varepsilon = 0.01$ and $c = \tanh(1)\sigma_0$; (a) corresponds to the case of *(i)*, and

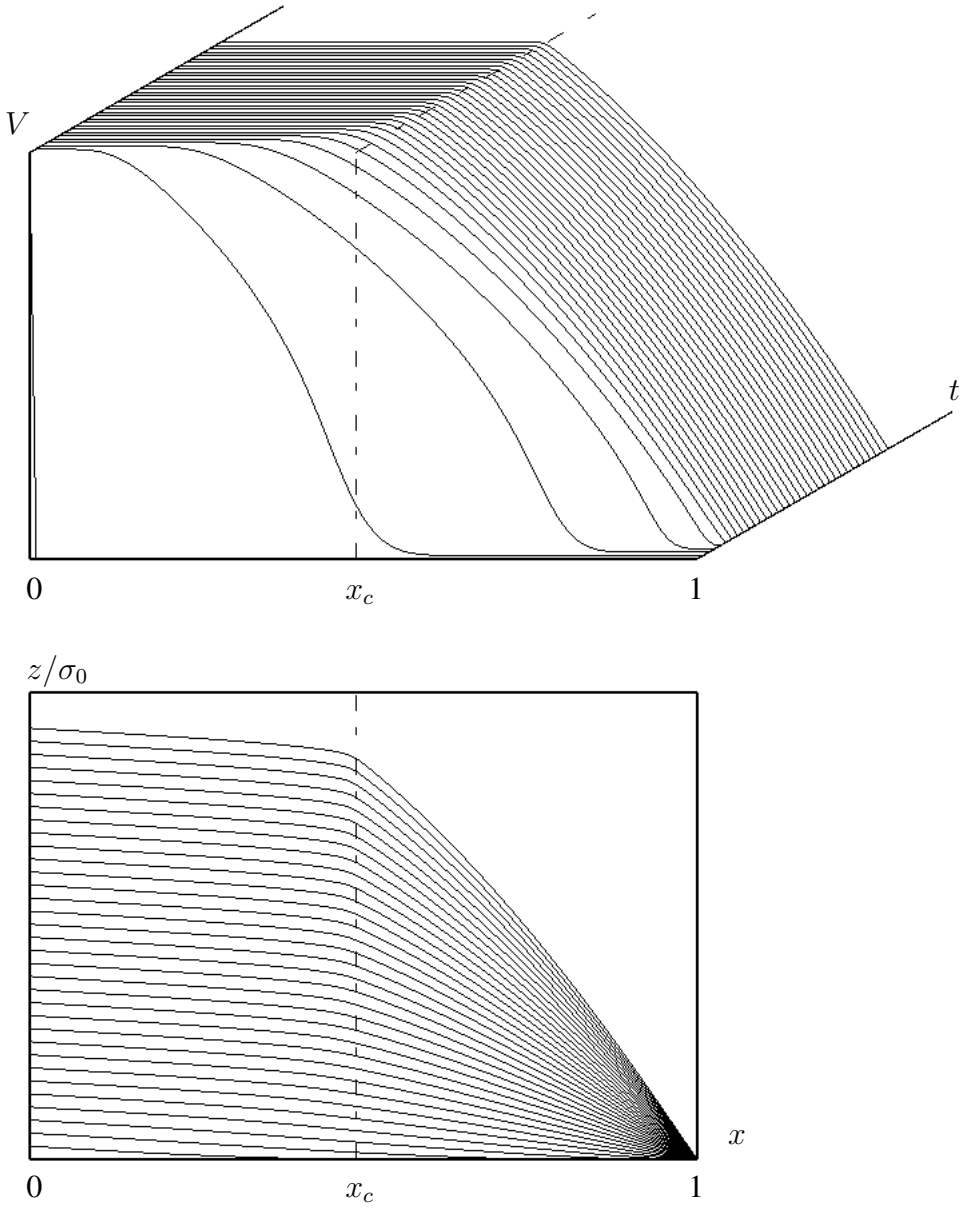

Figure 7: (b) corresponds to the case of *(ii)*.

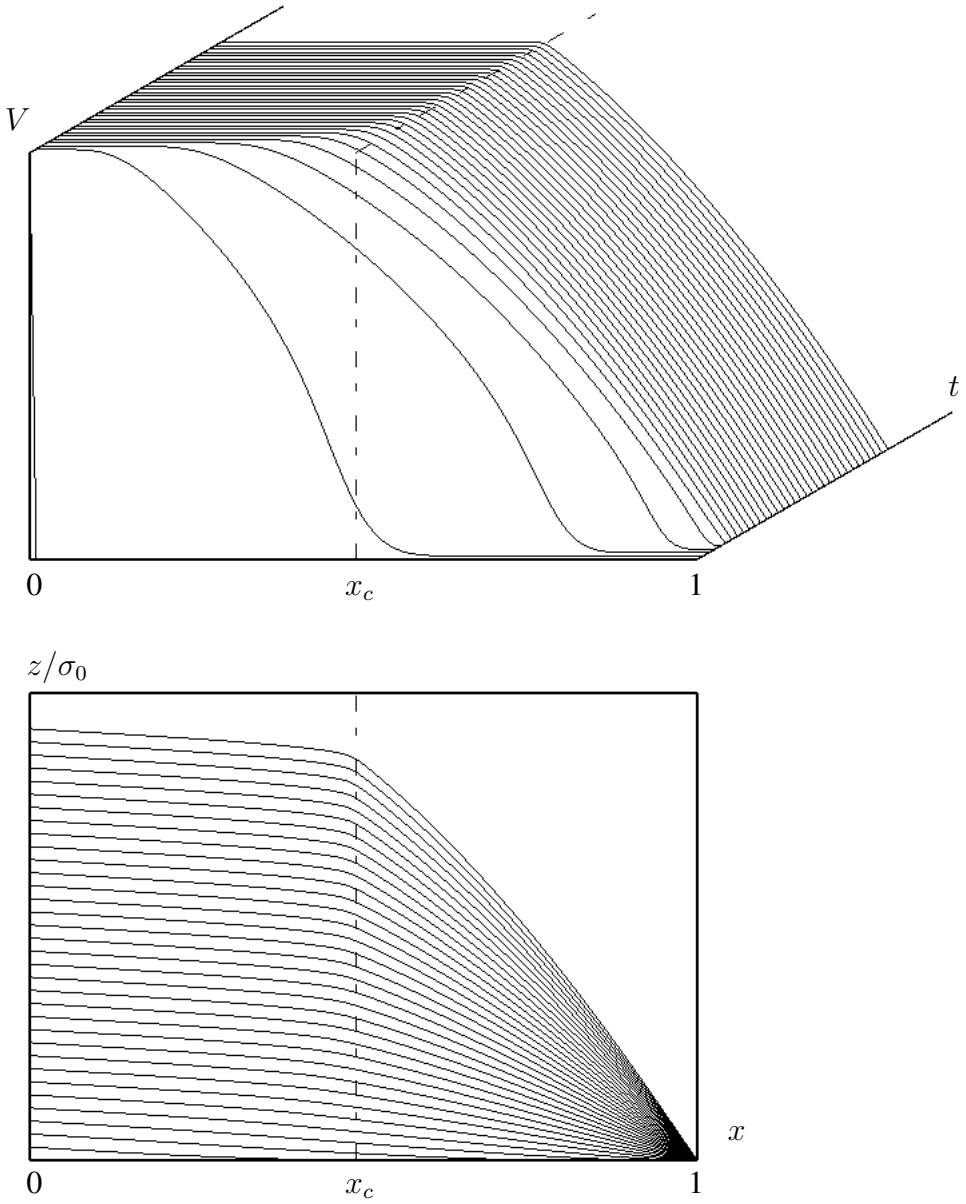

Figure 8: (a) The growth rates V as a function of x at various time instances t in the top figure, and the profiles of crystal, *i.e.*, the height $z = u(x,t)$ scaled by σ_0 in the bottom for the same conditions as for Figure 4, *i.e.*, $\sigma_0 = 0.001$, $\varepsilon = 0.001$ and $c = \tanh(1)\sigma_0$; (a) corresponds to the case of *(i)*, and

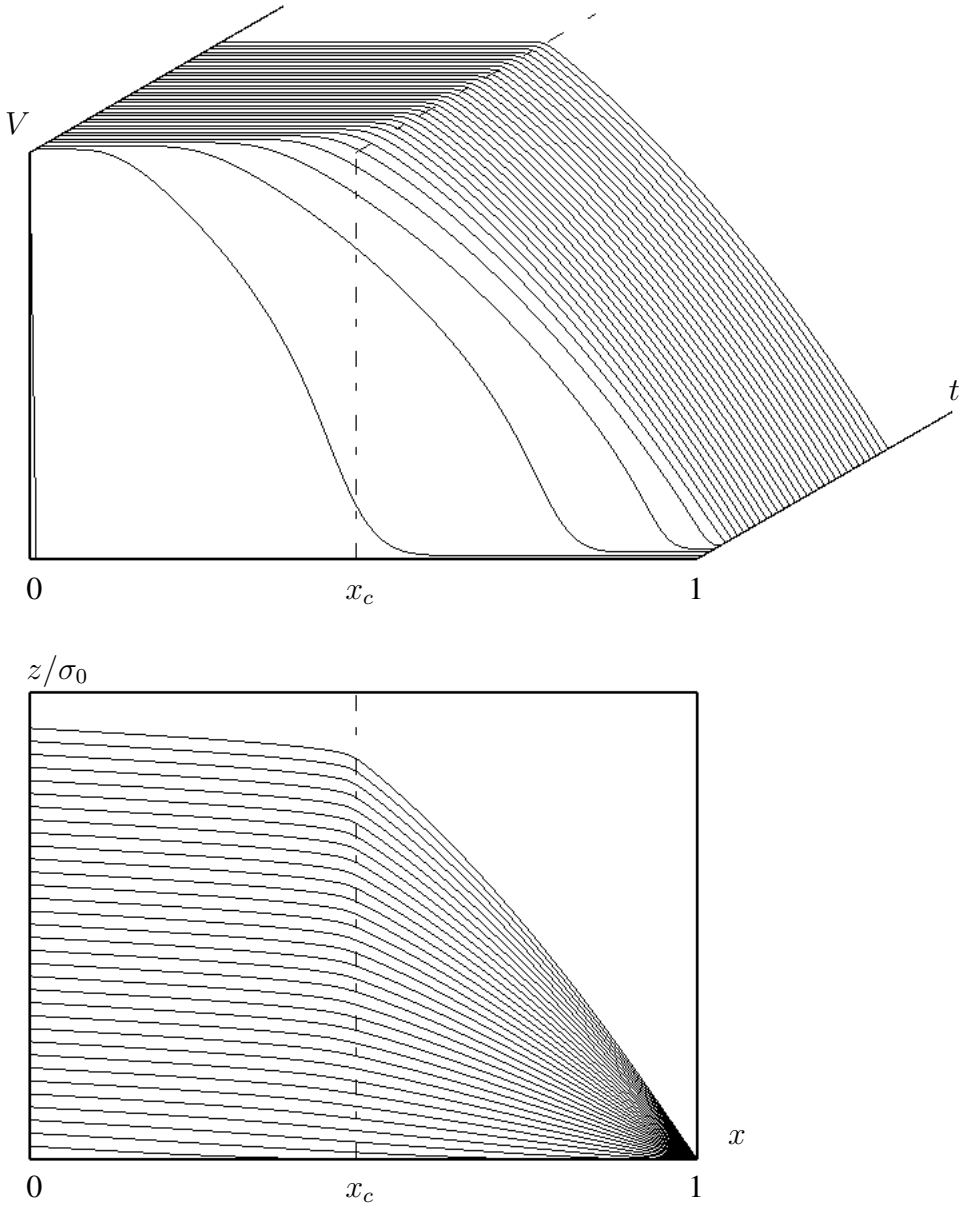

Figure 8: (b) corresponds to the case of *(ii)*.